CHALMERS

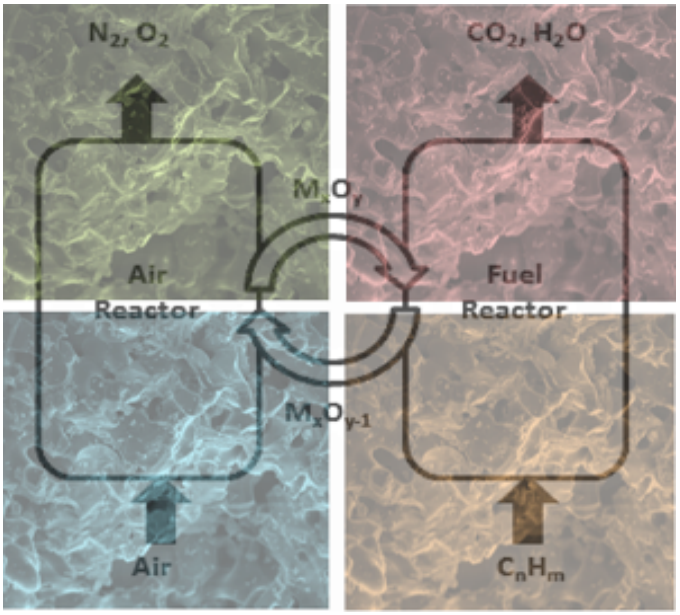

Production and examination of oxygen carrier materials based on different manganese ores with addition of calcium hydroxide or iron oxide in chemical-looping combustion

Master of Science Thesis in the Master Degree Programme, Sustainable Energy Systems

Nasim Mohammad Pour

Department of Energy and Environment
Division of Energy Technology
CHALMERS UNIVERSITY OF TECHNOLOGY
Göteborg, Sweden, 2013
Master Thesis 2013: T2013-383

Master Thesis 2013: T2013-383

Production and examination of oxygen carrier materials based on different manganese ores with addition of calcium hydroxide or iron oxide in chemical-looping combustion

Nasim Mohammad Pour

Department of Energy and Environment

Chalmers University of Technology

Göteborg, Sweden 2013

Production and examination of oxygen carrier materials based on different manganese ores with addition of calcium hydroxide or iron oxide in chemical-looping combustion

Master Thesis

NASIM MOHAMMAD POUR

Technical report nr: T2013-383

Department of Energy and Environment

Division of Energy Technology

Chalmers University of Technology

SE-412 96 Göteborg

Sweden

Telephone: + 46 (0)31-772 1000

Chalmers Reproservice

Göteborg, Sweden 2013

Report nr: T2013-383

Production and examination of oxygen carrier materials based on different manganese ores with addition of calcium hydroxide or iron oxide in chemical-looping combustion

NASIM MOHAMMAD POUR
Department of Energy and Environment
Division of Energy Technology
Chalmers University of Technology
SE-412 96 Göteborg, Sweden

Chemical-looping combustion (CLC) is an emerging method to capture carbon dioxide during combustion. It utilizes an oxygen carrier, normally particles of metal oxide, that is circulating between two fluidized bed reactors. One of the main challenges of this method is the cost of oxygen carries, which is composed of the cost of raw materials and the manufacturing cost. This study involves production of oxygen carriers by using six different manganese ores. Two additive materials, calcium hydroxide and iron oxide, were added to improve the characteristics of the ores. The method utilized to manufacture particles is extrusion, in which materials used for oxygen carrier preparation are mixed mechanically and extruded. The extrudates are then dried and sintered at high temperatures. Methane and syngas conversion as well as oxygen release in inert atmosphere were investigated for the oxygen carriers produced. Wood char conversion for three of the samples with addition of calcium hydroxide sintered at 1300°C for 6 hours as well as petroleum coke conversion of the three oxygen carriers with addition of iron oxide with manganese-iron molar ration of 1:2 sintered at 950°C for 4 hours were measured. The reactivity was improved for most of the manganese ores after the proposed treatments. Reactivity results of the oxygen carrier based on South African (B) manganese-ore sintered at 1300°C for 6 hours are the most promising ones among all the tested Mn-ore-based samples with addition of calcium hydroxide. Oxygen carrier manufactured from Brazilian ore with Mn/Fe molar ratio of 2:1 sintered at 950°C for 4 hours showed the best methane conversion among the all samples with addition of iron oxide.

Producing feasible oxygen carriers directly from ores would cut the cost of chemical looping combustion and could have a significant impact on its competitiveness among other carbon capture technologies.

Key words: CO_2 capture, Chemical-looping combustion, Oxygen carrier, Manganese ore, Calcium hydroxide, Iron oxide, Extrusion

Table of Contents

1. Introduction

Due to increasing destructive evidences of global warming in recent decades, the needs for carbon emission abatement has dramatically increased. The Kyoto protocol is an example of international negotiations to reduce anthropogenic greenhouse gas emissions[18]. The ecosphere has limited capacity to assimilate natural flows; increasing emission of greenhouse gases (GHG) like carbon dioxide and methane, and the accumulated concentrations of them, cause temperature rising by absorbing outgoing infrared radiation. Among GHGs, carbon dioxide is the main factor for global warming. The concentration of CO_2 has increased from 280 ppm in preindustrial era to almost 370 ppm today[24]. Burning fossil fuels, which make 80-85% of the primary energy of the world, is the main source of CO_2 emission. Although fossil fuels resources are known to be limited, still there are enough resources to threat the environment for centuries; so mitigating CO_2 is one of the key solutions for global warming problem. Carbon capture and storage (CCS) is known to be one of the most effective and long-term method to mitigate CO_2 emissions.

1.1. Carbon capture technologies

There are three well-known techniques for CO_2 capture; 1) Post combustion carbon capture, in which CO_2 is removed after the combustion, 2) Pre-combustion capture technologies that utilize gasification to separate carbon before combustion and 3) Oxyfuel combustion, in which fuel is burnt by oxygen instead of air.

1.1.1. Post combustion carbon capture technologies

In the post combustion carbon capture technologies CO_2 is removed from the outgoing flue gases after the combustion is completed [33].

Post combustion technologies can remove up to 90% of the CO_2 from the flue gases. However, for fossil fuel power plants with large flow rate of flue gases, these technologies would lower the total efficiency by about 10%. Another drawback of these methods is their high economic cost, which is about 30-50 USD per ton of captured CO_2[10].

1.1.2. Pre-combustion carbon capture technologies

In pre-combustion carbon capture technologies carbon is removed before the combustion takes place. For this purpose gasification is utilized, in which coal is gasified with steam or oxygen at high temperature and pressurized atmosphere. The product is known as syngas (CO/H_2). After removing the impurities in the syngas, a catalytic shift reactor the CO converts to CO_2 through a water-gas shift reaction (reaction 1) [14].

$$CO+H_2O \rightarrow H_2+CO_2 \quad (1)$$

Because the CO_2 concentration in the product flue gas is higher than in post-combustion, carbon capture in pre-combustion is cheaper. However the need for the shift reactor and other essential processes makes it more costly and causes significant energy penalty [10].

1.1.3. Oxyfuel combustion carbon capture technologies

In the oxyfuel combustion technique instead of air, fuel is combusted with pure oxygen. This excludes large amount of nitrogen in the flue gas that prevents NOx formation. The flue gas mostly contains CO_2, H_2O and small amount of nitrogen oxides (NOx) and sulfur dioxide (SO_2). H_2O is removed by condensation and after removing NOx and SO_2 nearly pure carbon dioxide is stored[14] .

Although in oxyfuel technologies costly separations techniques used in post combustion technologies are avoided, however, the need for an air separation unit (ASU) to gain nearly pure oxygen raises the costs and causes energy penalty.

Carbon storage

Like capturing, there are several options for storing carbon as well; geological, ocean and mineral storage are the three well-known options[26].

1.3. Chemical- Looping Combustion

The three mentioned methods for capturing carbon dioxide provide the possibility of reducing carbon emission but there are some drawbacks such as high-energy penalty and

high gas separation costs which lower the overall plant efficiency. Chemical-looping combustion (CLC) is an emerging method to capture carbon without the disadvantages of the pervious methods.

A CLC system includes two fluidized bed reactors (figure 1), a fuel reactor (FR) to which fuel is fed and where it reacts with the oxygen of an oxygen carrier, usually a metal oxide, (reaction 2), and an air reactor (AR) in which the reduced oxygen carrier is re-oxidized by air (reaction 3).

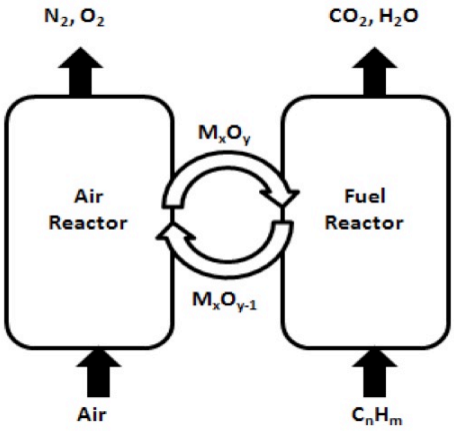

Figure 1- *Schematic representation of the chemical-looping combustion process*.

FR: $(2n + m)\ Me_xO_y + C_nH_{2m} \rightarrow (2n + m)\ Me_xO_{y-1} + mH_2O + nCO_2$ (2)

AR: $2Me_xO_{y-1} + O_2 \leftrightarrow 2Me_xO_y$ (3)

Considering which metal oxide is used, the reactions in the fuel reactor can be either endothermic or exothermic. On the other hand, reactions in the air reactor are always exothermic. The total amount of heat released from fuel reactor and air reactor is equal to the heat released from ordinary combustion. Therefore, separation of CO_2 by CLC does not cause any energy loss.

The outlet flows of the fuel reactor are CO_2 and H_2O. A condensation unit separates CO_2 from water vapor. In the air reactor the oxygen reacts with the reduced metal oxide

(Me_yO_{x-1}) and high temperature N_2 and un-reacted O_2 leave the reactor. The high temperature gas from the air reactor can be used in a gas turbine cycle to generate power and afterwards it is released into the atmosphere with no harm to the environment.

The most important advantage of the CLC technique is that CO_2 and H_2O are inherently separated from other flue gases, which makes the carbon capture possible with no direct energy penalty. Since air and fuel in CLC are led to separate reactors, combustion takes palce withot any falme. So thermal formation of NOx is naturally avoided which makes CLC an even more attarctive environmental friendly option[21].

1.4. Chemical-Looping with Oxygen Uncoupling (CLOU)

For combusting of solid fuels in CLC there is usually the necessity of a gasification stage in which the solid fuel is gasified with steam or CO_2. This step often slows down the reaction rate and thereby increases the overall costs. There is another option known as chemical-looping with oxygen uncoupling (CLOU)[20]. In this method an oxygen carrier releases gaseous O_2 in the fuel reactor. Thereby, fuel particles can react directly with gas-phase oxygen. CLOU includes three steps; one in the air and two in the fuel reactor. In the first step in the fuel reactor the oxygen carrier releases its oxygen (reaction 4), in the second step the gas-phase O_2 reacts with gaseous fuel (reaction 5) or solid fuel (reaction 6) and during the third step the reduced oxygen carrier is re-oxidized with oxygen in the air reactor (reaction 6).

Reactions in the fuel reactor:

$Me_xO_y \leftrightarrow Me_xO_{y-2} + O_2\,(g)$ (4)

$C_nH_{2m} + (n + m/2)\,O_2(g) \rightarrow nCO_2 + mH_2O$ (5)

$C + O_2\,(g) \rightarrow CO_2$ (6)

Reaction in the air reactor:

$O_2\,(g) + Me_xO_{y-2} \leftrightarrow Me_xO_y$ (7)

The reactions 4 and 7 are the same reactions in opposite directions so they cancel each other and the net reaction would be the reactions 5 or 6 which is similar to CLC or to normal combustion.

1.5. Oxygen carriers

Oxygen carriers play a very important role in CLC technique, therefor manufacturing and selecting them will influence significantly on the costs and total efficiency of a CLC system.

Oxides of metals like copper, manganese, nickel and iron have been used by many CLC researches [9,13, 29].

Although selection of oxygen carriers depends on the fuel and the conditions of the system, there are some general criteria that should be considered. Thus oxygen carriers should:

- Be highly reactive both in reduction and oxidation reactions
- Be highly resistant to fragmentation, attrition and agglomeration
- Have minimum production cost and environmental impacts
- Have high oxygen transfer capacity
- Have suitable fluidization characteristics during high temperatures in redox cycles.

Economic costs

Overall cost of oxygen carrier production is an important factor that should be considered. The production cost for a synthetic oxygen carrier includes cost of metal oxide and inert materials plus manufacturing cost. Two important parameters to investigate and compare for the cost of different oxygen carriers are reactivity and lifetime. For example producing a rather expensive oxygen carrier with very long lifetime and high reactivity can be more economical than to produce a rather cheap one with short lifetime and low reactivity. Lifetime of oxygen carriers is defined as the average time that a particle undergoes redox cycles without losing its reactivity and mechanical strength[1].

As it is shown in figure 2 among the metal oxides used for oxygen carrier production, cobalt and nickel are the most expensive and manganese and iron are among the cheapest ones[1].

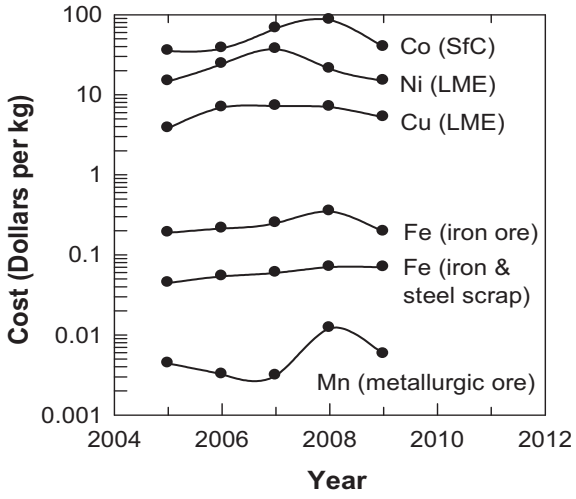

Figure 2- *Average annual cost of materials used for oxygen-carriers preparation. SfC: spot for cathodes; LME: London Metal Exchange*[1]*.*Cost of Mn ore in this figure doesn't seem realistic, Its price is probably based on dollar per DMTU (dry metric ton unit). To correct it, the costs of Mn in this figure should be multiplied by contained manganese in Mn ore (45-50%) and 100. e.g., cost of Mn ore in 2008 would be: 0.012*100 *50%=0.6 $ per kg. Thus the graph for Mn ore would be above Fe's.*

Environmental aspects

Another consideration of materials used as oxygen carrier is their environmental impacts. Environmental studies have shown that cobalt and nickel may cause some health risks such as cancer. On the other hand, iron and manganese are considered to be non-toxic materials.

Carbon deposition

Carbon deposition occurs when the carbon travels with the oxygen carrier particles from the fuel reactor to the air reactor and burns there. This phenomenon depends on the metal oxide, the inert material and the H_2O/fuel ratio. Availability of oxygen is a factor that can affect carbon deposition. Generally, carbon deposition can be avoided by modifying the reactor system design.

Agglomeration

Agglomeration is a phenomenon that happens when the particles stick together. This would reduce fluidizability of the bed materials in the reactor. Which type of support materials, combination of metal content, calcination conditions and operational conditions are some of parameters that affect agglomeration of the oxygen carriers.

Attrition

Attrition happens when oxygen carrier particles are degraded due to friction, erosion or high temperature. It is an important parameter that shows resistance of particles against chemical and physical stresses during reduction/oxidation reactions. Crushing strength is an indicator of the tendency of particles toward attrition. Normally particles with crushing strength below 1 N are known to be so soft and easier to attrite.

1.6. Manganese-based oxygen carriers

Manganese oxide is a good oxygen carrier candidate due to its low price, comparably high reactivity and non-toxicity. It also shows higher oxygen transport capacity in comparison with other cheap candidates like iron [1]. Among several manganese oxides MnO_2 and Mn_2O_3 have the highest oxidization capacity but they are highly unstable and very likely to decompose at CLC working temperature range (850-950°C). Moreover, there is thermodynamic restriction in the oxidation phase for regeneration of these oxides [23]. As it can be seen in the figure 3, in the air reactor with maximum 5% O_2 partial pressure Mn_2O_3/ Mn_3O_4 can only be oxidized at temperature below 800°C. On the other hand, Mn_3O_4 shows more stability at higher temperatures, so in CLC experiments the phase transition is likely to be between Mn_3O_4 and MnO[30]. However, during redox cycles phase transition of Mn_3O_4 to MnO would lead to significant change in density, which results in lowering the mechanical strength[12].

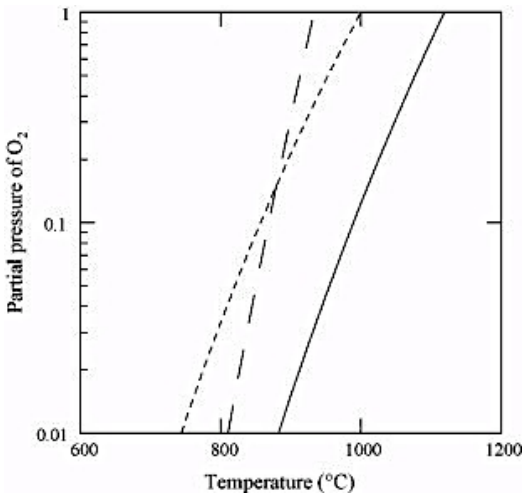

Figure 3-*The partial pressure of gas-phase O_2 over the metal oxide systems CuO/Cu_2O(—), Mn_2O_3/Mn_3O_4 (- - - - -) and Co_3O_4/CoO (— —) as a function of temperature*[23]

Several support materials have been investigated to improve the reactivity and mechanical strength of pure manganese oxides. Johansson et al. investigated ZrO_2 as support for Mn_3O_4[16]. The drawback of using zirconia as support is the risk of phase transition (monoclinic to tetragonal), which causes cracks in its structure. To overcome this problem and stabilize ZrO_2 they applied several oxides like CaO, MgO, CeO_2 or Y_2O_3[16].

Manganese-based oxygen carriers have been considered for CLOU applications as well. Applying pure manganese oxide in CLOU is troublesome because the relevant equilibrium concentrations applicable for CLOU with Mn at relatively low temperatures. However, combining manganese oxide with other materials can raise the temperature. Iron, nickel, silicon, magnesium and calcium are examples of materials that can be combined with manganese oxides to change its characteristics. For instance, the CLOU effect of Fe-Mn-based oxygen carriers with gaseous and solid fuel in a small fluidized bed batch reactor was tested by Azimi et al.[5]. Shulman et.al tested manganese oxides with MgO and addition of TiO_2 and $Ca(OH)_2$[29]. Titania was added to prevent decompositions of the manganese based spinel and the addition of calcium hydroxide is to produce manganese-based perovskite structures with calcium contents that have a higher CLOU effect [29]. Perovskite $CaMnO_{3-\delta}$ compositions are known to have high oxygen capacity and stable structure at highly oxygen non-stoichiometry[11]. Pure Mn-oxides during the oxygen

up-taking and releasing in CLC/CLOU cycles are likely to sinter and agglomerate. That mostly happens due to high temperature during redox cycles, which is needed since cation diffusion mechanism is dominant. In this condition the caking and oxygen uptake or release occur at the same temperature. In order to decrease the needed temperature for oxygen uptake/release, instead of Mn-oxide, perovskite phases of Ca-Mn-O ($CaMnO_{3-\delta}$) are introduced. In this compositions, instead of cation diffusion, oxygen diffusion is the main mechanism during redox cycles [17]. This characteristic of pervoskite ($CaMnO_{3-\delta}$) is an interesting candidate for CLOU applications. Rydén et al. examined CLOU effect of perovskite $CaMn_{0.875}Ti_{0.125}O_3$, which showed decent gas phase oxygen release [22].

In recent years the possibility of using manganese ores as oxygen carriers has been studied. Although manganese ore contains impurities that can affect its physical and chemical behaviour during redox cycles, it is cheaper than pure manganese oxides and in some cases has shown promising results[19, 12, 27] .

1.7. Oxygen carrier manufacturing methods

The method of material preparation has significant impact on the oxygen carrier properties. Shapes of particles, distribution of active metal oxide on the support material, reactivity and mechanical strength during redox cycles are some of the parameters that are influenced by the preparation method. Another important factor is the economic cost of manufacturing that can be a significant share of the cost of the process[1]. Particle manufacturing normally include three major steps; mixing and homogenization, formation of particles and particles calcination.

Mixing and homogenization

To homogenize the mixture several methods are utilized. In some methods like milling and rotary evaporation, powders of metal oxide and support materials are mixed mechanically. In another category of mixing, techniques like Co-precipitation, dissolution, sol-gel and solution combustion raw materials are mixed in an aqueous solution [8, 32, 28].

Formation of particles

In this step particles are formed by dispersing the well-homogenized slurry into hot air/nitrogen (Spray drying and Spin-flash drying) or into liquid nitrogen (freeze granulation) or by extruding the homogenized dough of materials in a cylinder syringe (extrusion) [15, 8, 2, 7].

Calcination of particles

In order to harden the particles and ensure formation of the desired phases, the particles are calcined at high temperature. This is done in the same way for different methods regardless of the previous steps.

1.8. Objective

The aim of this work is to test the CLC and CLOU properties of the oxygen carriers based on manganese ores with addition of calcium hydroxide or iron oxide prepared by an extrusion method.

2. Experimental

2.1. Oxygen carrier manufacturing method

The oxygen carriers were prepared by a simple extrusion method. In this method manganese ore and $Ca(OH)_2$ or iron oxide (Fe_2O_3) were mixed mechanically. All the used ores contain some iron and it is very likely that iron substitutes for manganese in reacting with $Ca(OH)_2$. In order to assure formation of the favourable phase a stoichiometric amount of $Ca(OH)_2$ or Fe_2O_3 was therefore added relative to the sum of Mn+Fe in the ore. To obtain a well-homogenized mixture wet ball milling was applied. Distilled water was added to the mixture of Mn-ore and $Ca(OH)_2$ or Fe_2O_3 powders (particle size<90μm). The slurry was milled in an alumina jar with small stainless steel balls for 2 hours. The homogenized slurry was put into an oven set to 200°C to be dried overnight. In order to get the best result in terms of viscosity, particle size and particle distribution, polyvinyl alcohol as binder, quaternary ammonium compound as dispersant, ammonium hydroxide as peptizing agent and distilled water as solvent were added to the dried mixture. The well-mixed dough was extruded using a hand-held single-screw manual extruder. The extrudates were collected on a stainless steel plate and put into oven set to 200°C to be dried overnight. Hedayati et al. used a more elaborate version of this method, rotary evaporator, to homogenize the mixture to manufacture ceria-supported oxygen carriers [3].

In order to find the most optimal sintering scheme, several samples from each Mn-ore were made and calcined at different temperature/duration. Detailed information about different samples with addition of $Ca(OH)_2$ is presented in Table 1. The denotation of the samples follows a general pattern, in which the three or four first letters present an abbreviation of the Mn-ore name, the following four digits show sintering temperature and the last digits present the sintering duration in hours. Having several Mn-ores with different compositions and applying the simple method to manufacture the particles, brought the necessity to have a reference particle as a basis to evaluate the manufacturing method. This reference oxygen carrier was made from synthetic manganese oxide (Mn_2O_3) and $Ca(OH)_2$, and was denoted as SMN.

Table 1- *Denotation and calcination schemes of manufactured samples with addition of $Ca(OH)_2$*

Samples	ID	Calcination temperature (°C)/duration(h)
Mn_2O_3/ $Ca(OH)_2$	SMN13006	1300/6
	SMN12006	1200/6
Gabon Mn-ore/ $Ca(OH)_2$	GBN13006	1300/6
	GBN12006	1200/6
East European	ESE13006	1300/6
Mn-ore/ $Ca(OH)_2$	ESE12506	1250/6
	ESE120012	1200/12
	ESE12006	1200/6
South African(A) Mn-ore/$Ca(OH)_2$	SAFA13006	1300/6
	SAFA120012	1200/12
	SAFA12006	1200/6
South African(B) Mn-ore/$Ca(OH)_2$	SAFB13006	1300/6
	SAFB12506	1250/6
	SAFB12006	1200/6
Brazilian Mn-ore/Ca(OH)2	BRZ13006	1300/6
	BRZ12012	1200/12
Egyptian Mn-ore/Ca(OH)2	EGP13006	1300/6

Five different samples based on the four ores and Fe_2O_3 with Mn:Fe molar ratio of 1:2 were made and tested, which are presented in Table 2. In each sample ID the first three or four letters present an abbreviation of the Mn-ore name, the following digit shows the Mn:Fe molar ratio, F represents iron oxide, the following four digits show sintering temperature and the last digits present the sintering duration in hours.

Some experiments were done with the South African (A) and Egyptian ores, (SAFA2F100012110012 and EGP2F100012110012). During the preparation procedure of these particles with Mn:Fe molar ratio of 1:2, after milling, the particles were put into an oven set to 1000°C for 12 h. The sintered mixture was extruded afterwards and calcined at 1100°C for 12 hours.

Table 2- *Denotation and calcination schemes of manufactured samples with addition of Fe_2O_3*

Samples	**ID**	**Molar ratio(Mn:Fe)**	**Sintering temp (°C)/time (h)**
East European Mn-ore/ Fe_2O_3	ESE2F11006	1:2	1100/6
South African(A) Mn-ore/ Fe_2O_3	SAFA2F100012110012	1:2	1000/12 +1100/12
South African(B) Mn-ore/ Fe_2O_3	SAFB2F11006	1:2	1100/6
Egyptian Mn ore/ Fe_2O_3	EGP2F100012110012	1:2	1000/12 +1100/12
	EGP2F1000129504	1:2	1000/12 +950/4

Based on the results of experiments with the samples in Table 2, oxygen carriers based on the six manganese ore and addition of Fe_2O_3 with two different Mn/Fe molar ratios were made. The results are presented in Table 3. All of these samples were sintered at 950°C for 4 hours. The denotation of the samples presented at the Table 3 is the same as those at Table 2. The only difference is that the digit standing for the Mn:Fe molar ratio comes at the beginning of the ID.

Table 3- *Denotation and calcination schemes of manufactured samples with addition of Fe_2O_3, all sintered at 950℃ for 4 hours.*

Samples	ID	nMn/nFe	Calcination temperature (°C)/duration(h)
Gabon Mn-ore/ Fe_2O_3	GBN2F9504	1/2	950/4
	2GBNF9504	2/1	950/4
East European Mn-ore/ Fe_2O_3	ESE2F9504	1/2	950/4
	2ESEF9504	2/1	950/4
South African(A) Mn-ore/ Fe_2O_3	SAFA2F9504	1/2	950/4
	2SAFAF9504	2/1	950/4
South African(B) Mn-ore/ Fe_2O_3	SAFB2F9504	1/2	950/4
	2SAFBF9504	2/1	950/4
Brazilian Mn ore/ Fe_2O_3	BRZ2F9504	1/2	950/4
	2BRZ2F9504	2/1	950/4
Egyptian Mn ore/ Fe_2O_3	EGP2F9504	1/2	950/4
	2EGPF9504	2/1	950/4

After calcination, extrudates were crushed and sieved. Particles in the size range of 125-250 μm were collected and used in the experiments. In this study oxygen carriers manufactured from six different Mn-ore were examined. Each Mn-ores has its own composition and impurities, which could lead to formation of complex chemical phases. So each ore shows different physical and chemical behaviour during CLC/CLOU

processes. In Table 4 composition analysis of the all used manganese ores is presented.

Table 4 –*Elemental Composition analysis of manganese ores in wt%*

ELEMENT	Egyptian	East European	Gabon	South African A	South African B	Brazilian
Si	2.13	7.07	5.19	0.84	2.63	5.84
Al	0.58	0.24	3.26	0.20	0.17	4.05
Ca	10.15	6.76	0.37	4.12	5.42	0.21
Fe	15.95	5.76	4.92	18.61	13.08	5.61
K	0.10	0.35	0.37	0.07	0.04	0.52
Mg	0.93	1.71	0.01	0.47	0.65	0.40
Mn	37.80	48.26	49.11	44.30	49.03	53.29
Na	0.41	0.32	0.05	0.06	0.04	0.04
P	0.06	0.03	0.50	0.04	0.03	0.06
Ti	0.03	0.03	0.10	0.02	0.01	0.40

To have a better basis to evaluate the manufactured oxygen carriers' characteristics, the six pure manganese ores without any pre-treatment were tested under the same experimental conditions.

2.2. Experimental set up

All the experiments were performed in a straight fluidized bed reactor with a total length of 820 mm and with a quartz porous plate of 22 mm in diameter placed 370 mm from the bottom. Two Pentronic CrAl/NiAl thermocouples enclosed in quartz tubes inside the reactor measured the temperature 5 mm under and 10 mm above the porous quartz plate. The temperature presented in this work is the set-point temperature, i.e. the temperature at the beginning of the reduction, measured by the upper thermocouple.

For experiments with gaseous fuel, a sample of 10 g of oxygen carriers with the size of 125-250 μm was placed on the porous plate. The reactor was then heated up to 900°C in a 900 mL_n/min flow of 5% O_2 in nitrogen (oxidation period). When particles were adequately oxidized they were fluidized by 600 mL_n/min of pure N_2 (inert period). The particles were exposed to consecutive cycles of oxidizing and inert periods at a temperature of 900°C. For reactivity evaluation, the particles were exposed to 450 mL_n/min of CH_4 or syngas (50/50% H_2/CO) at 950°C. The oxidation and the reduction periods were separated by 60 sec of inert periods, in which N_2 is passed through the reactor. The introduction of N_2 purged the reactor from the product gases of the CH_4 or syngas period and oxygen of the oxidation period. Details of the experimental scheme are presented in Table 5.

Table 5- *Experimental scheme for gaseous fuel; ox, in, and red stand for oxidation, inert and reduction respectively.*

No of cycles	Reducing gas	F_{ox} (mL/min)	F_{in} (mL/min)	F_{red} (mL/min)	t_{in} (s)	t_{red} (s)	T_{ox}	T_{red}
3	Nitrogen	900	600	-	360	-	900	900
n	Methane	900	600	450	60	20	950	950
2	Syngas	900	600	450	60	80	950	950
3	Nitrogen	900	600	-	360	-	900	900

For solid fuel experiments, a sample of 10 g oxygen carrier particles with a size of 125–250 μm was placed onto the porous plate and heated to the temperature of interest in a flow of 1000 mL_n/min of a gas mixture consisting of 5% O_2 and 95% N_2. The particles were then alternatingly exposed to this O_2/N_2 mixture, and a reducing period in which 0.3 g of wood char or devolatilized petroleum coke was introduced to the bed of oxygen carrier particles. During reducing periods the reactor was fluidized with 900 mL_n/min of pure N_2. Further, 300 mL_n/min of inert sweep gas, that is, N_2, was also introduced to the system at the top of the reactor together with the solid fuel throughout the reducing period to ensure that the pulverized fuel did not get stuck in the feed line. This sweep gas did not enter the hot reaction zone of the reactor. The oxidation and the reduction periods were separated by an inert period with 900 mL_n/min of pure N_2 for 60 s. In order to verify reproducibility, all solid fuel experiments were carried out three times each. The solid fuel used for these tests were Swedish wood char [6] or devolatilized petroleum coke, which their analysis is reported in Table 6.

Table 6-*Soild fuels analysis*

	Proximate [wt%, as received]		[wt%d.a.f]	Ultimate [wt%,d.a.f]				
Fuel	**Moisture**	**Ash**	**Volatiles**	**C**	**H**	**N**	**S**	**O**
Wood Char	3	3	11	83	-	-	-	-
Devolatilized Petroleum coke	0.5	0.8	10.9	88.4	2.3	1.93	6.459	0.5

All the exhaust gases from the reactor passed through an electric cooler and after condensation of H_2O, the flue gas was led to a gas analyzer (Rosemount NGA-2000), which measured the concentration of CO, CO_2, H_2, O_2 and CH_4 (see figure 4). From high frequency measurements of the pressure drop it was possible to see if the bed was fluidized or not.

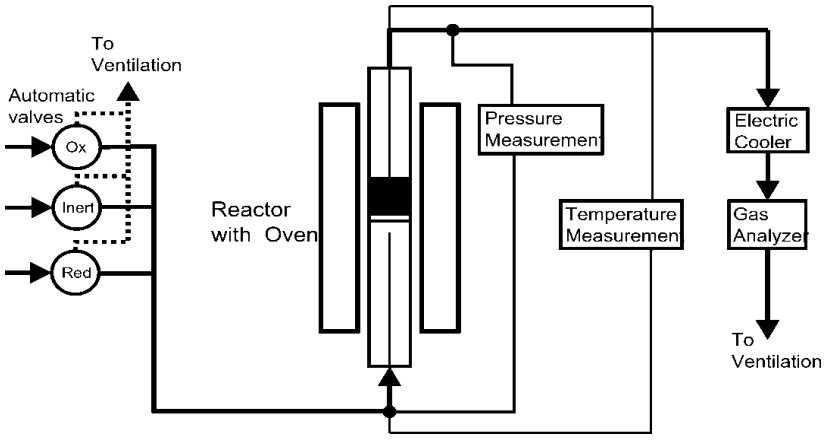

Figure 4- *Scheme of the experimental setup*

2.3. Data Evaluation

Oxygen carrier's conversion is evaluated by using mass based conversion, ω, which is defined as the actual mass of oxygen carrier, m, divided by the mass of oxygen carrier in the most oxidized state, m_{ox} (equation 8).

$$\omega = \frac{m}{m_{ox}} \qquad (8)$$

When CH_4 (equation 9) or syngas (equation 10) is used as fuel, ω is calculated as a time integral using measured outgoing gas concentrations.

$$\omega_i = \omega_{i-1} - \int_{t_0}^{t_1} \frac{\dot{n}_{out} M_O}{m_{ox}} (4P_{CO_2} + 3P_{CO} + 2P_{O_2} - P_{H_2}) dt \quad (9)$$

$$\omega_i = \omega_{i-1} - \int_{t_0}^{t_1} \frac{\dot{n}_{out} M_O}{m_{ox}} (2P_{CO_2} + P_{CO} + 2P_{O_2} - P_{H_2}) dt \quad (10)$$

In the N_2 periods ω is calculated as a time integral of outgoing O_2 concentration (equation 11).

$$\omega_i = \omega_{i-1} - \int_{t_0}^{t_1} \frac{2\dot{n}_{out} M_O}{m_{ox}} P_{O_2} dt \qquad (11)$$

In the solid fuel experiments the mass based conversion during reduction with wood char or petroleum coke is described by means of equation 12.

$$\omega_i = \omega_{i-1} - \int_{t_0}^{t_1} \frac{2\dot{n}_{out} M_O}{m_{ox}} \Big(P_{CO_2} + 0.5P_{CO} + P_{O_2} - ((\frac{O_2}{C})_{fuel} \times (P_{CO_2} + P_{CO} + P_{CH_4})) + (0.5(\frac{H_2}{C})_{fuel} \times (P_{CO_2} + P_{CO} + P_{CH_4})) - 0.5H_2 - CH_4 \Big) dt \qquad (12)$$

Where ω_i is the mass conversion as a function of time for a period i, ω_{i-1} is the degree of conversion after the foregoing period; t_0 and t_1 are the times for the start and the end of the period. P_{CO2}, P_{CO}, P_{H2}, P_{CH4} and P_{O2} represent outlet partial pressures of the gases CO_2, CO, H_2, CH_4 and O_2 after removal of water vapour. M_O represents the molar mass of oxygen and $\dot{n}_{out}$ stands for the molar flow rate of the exhaust gas after condensation of H_2O. $(O_2/C)_{fuel}$ and $(H_2/C)_{fuel}$ are the estimated molar ratios of oxygen and hydrogen over carbon in the fuel.

Gas yield (γ) is defined as the fraction of CO_2 in the outlet gas flow divided by the sum of the outgoing carbon-containing gases on dry basis (equation 13). By this definition a gas yield of 1 means complete conversion of the gas fuel to CO_2.

$$\gamma = \frac{P_{CO_2}}{P_{CH_4}+P_{CO_2}+P_{CO}} \qquad (13)$$

3. Results

3.1. Gas conversion

The reactivity of the oxygen carriers to convert gaseous fuels was investigated by exposing them to a reducing atmosphere using CH_4 or syngas as described in section 2.2.

3.1.1. Gas conversion of the pure manganese ores

The ability of the six pure ores to convert CH_4 was tested. Figure 5 presents the gas yield, γ, as a function of oxygen carrier conversion, ω, during reduction with CH_4 as fuel at 950°C for the six pure, untreated manganese ores.

As illustrated in figure 5, East European ore, ESE, showed a quit decent methane conversion. During the 20 s of CH_4 period, this ore could release oxygen equivalent to $\Delta\omega = 1\%$ (see 3.2.1 below) . The other ores were not as reactive as ESE. Egyptian, South African A& B ores (EGP, SAFA and SAFB) had similar methane conversion indications. That could be due to the noticeable similarities in their compositions; all of these three ores have considerable share of Fe (see Table 4). Brazilian and Gabon ores (BRZ, GBN) showed the lowest conversion. Looking at Table 4, one could see these two have very similar compositions with considerable amount of Si and Al.

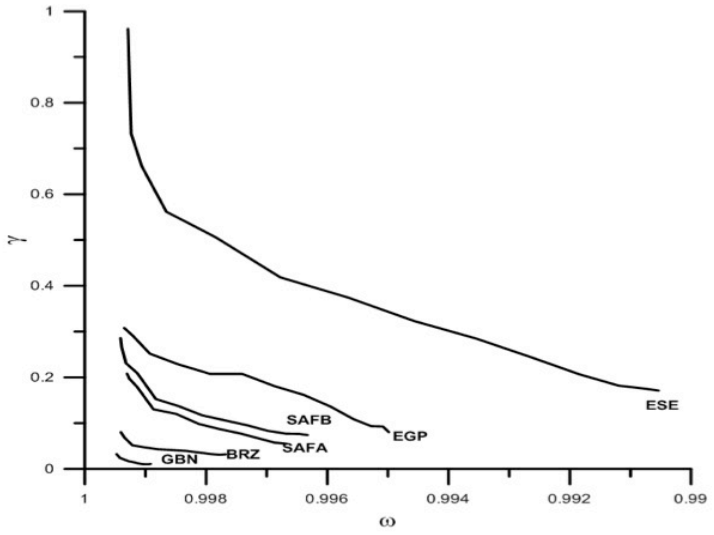

Figure 5- *Gas yield as a function of oxygen carrier conversion during reduction with CH_4 as fuel at 950°C for the six pure, untreated manganese ores*

3.1.2. Gas conversion of oxygen carriers with addition of $Ca(OH)_2$

Figure 6 presents the gas yield, γ, as a function of oxygen carrier conversion, ω, during reduction with CH_4 as fuel at 950°C for the five samples of manganese ore with addition of $Ca(OH)_2$ calcined at 1300°C/6h. As shown, the sample from synthetic manganese oxide, SMN13006, shows the highest conversion. This is quite expected and could be explained by the absence of impurities that results in complete formation of perovskite $CaMnO_{3-\delta}$. Among all the Mn-ore-based samples, South African (B) ore-based oxygen carrier, SAFB13006, showed the highest CH_4 conversion. On the other hand, Gabon ore-based sample, GBN13006, showed the lowest gas conversion.

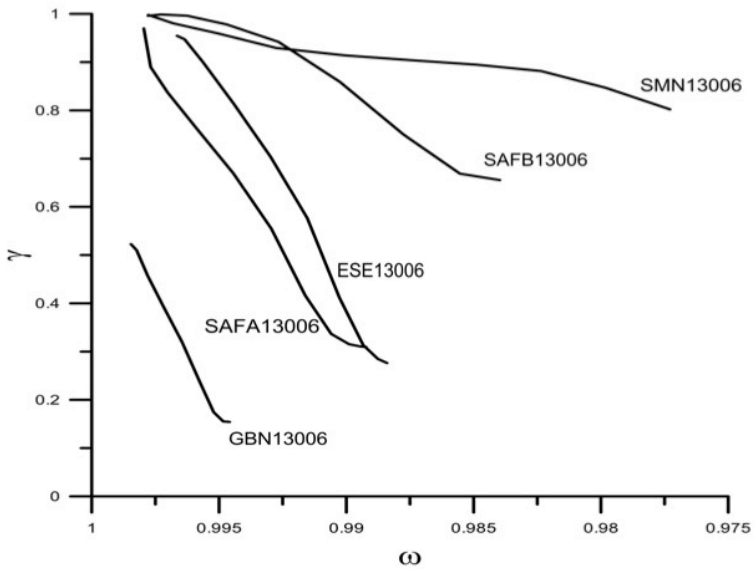

Figure 6-*Gas yield as a function of oxygen carrier conversion during reduction with CH_4 as fuel at 950°C for the five samples of manganese ore with addition of $ca(OH)_2$ calcined at 1300°C/6h.*

The sample based on Brazilian ore (BRZ13006) melted during calcination at 1300°C/6h and the Egyptian ore-based sample sintered at 1300°C/6h (EGP13006) was very soft and defluidized permanently during heat up. So, results of these two samples are not presented in the figure 6. The oxygen carriers made of each Mn-ore sintered at different schemes have different conversion trends (see figure 7). As seen in figure 7-a, among the oxygen carriers based on South African (B) ore, the gas yield of the sample calcined at 1300°C/6h, SAFB13006 has higher conversion than the other samples sintered at lower temperatures. The main phase of these particles was detected as cubic $CaMn_{(1-x)}Fe_xO_{3-\delta}$. Seemingly, the higher sintering temperature raises the methane conversion ability of these particles. All the SAFBs showed proper fluidization during the tests. On the other hand, as it is shown in figure 7-b these South African (B) ore-based oxygen carriers had the equal reactivity in terms of syngas conversion.

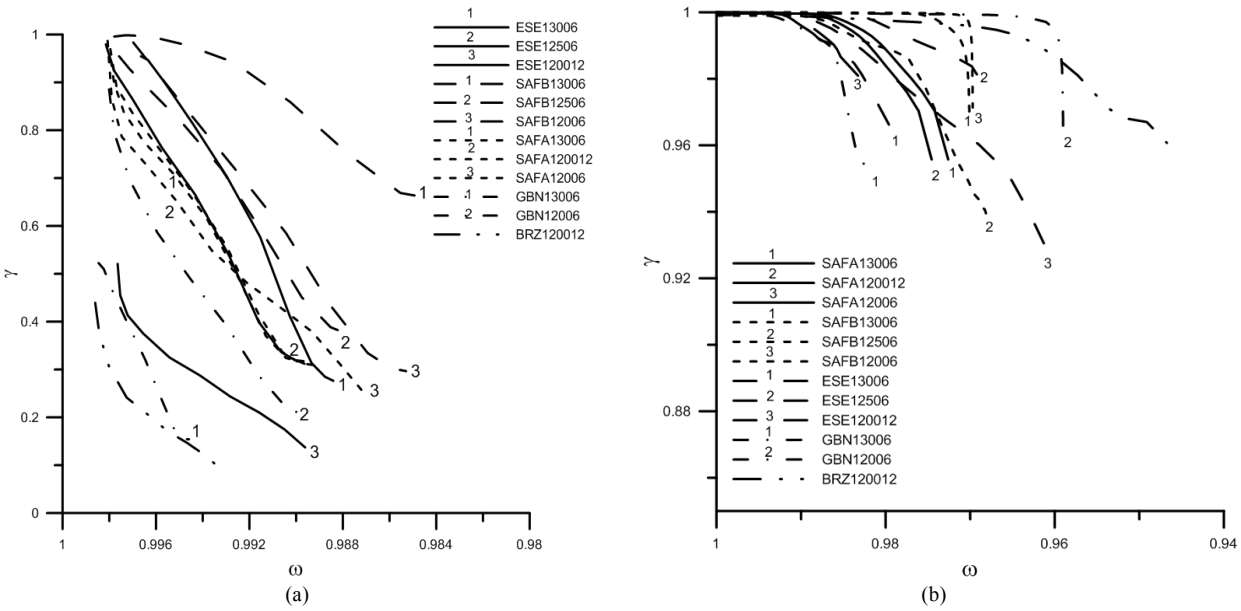

Figure 7- *Gas yield as a function of oxygen carrier mass-based conversion during reduction with (a) CH_4 and (b) syngas as fuel at 950°C*

For the SAFAs particles, methane and syngas conversion does not seem to be influenced by the calcination scheme. The South African (A) based oxygen carriers sintered at 1300°C/6h, 1200°C/12h and 1200°C/6h (SAFA13006, SAFA120012 and SAFA12006 respectively) had very similar gas conversion characteristics (see figure 7). All the SAFAs showed proper fluidization behaviour during the experiments and the main detected phase was in all cases cubic $CaMn_{(1-x)}Fe_xO_{3-\delta}$.

As seen in Table 1, the only ore examined at all sintering schemes is the East European ore. As shown in figure 7-a, CH_4 conversion of the East European ore–based samples calcined at 1300°C/6h and 1250°C/6h (ESE13006 and ESE12506) was almost the same. On the other hand, East European ore based oxygen carrier sintered at 1200°C/12h (ESE120012) showed lower reactivity in terms of CH_4 conversion. As illustrated in figure 7-b, the ESE12506 shows higher reactivity than ESE13006 and higher than ESE120012. The ESE-samples sintered at 1200°C (ESE120012 and ESE12006) had tendencies toward defluidization during fuel cycles. In the case of ESE12006 defluidization was so severe that no experiments with fuel could be done.

The Gabon ore-based samples, GBNs, showed considerable change in behaviour depending on the calcination scheme. As illustrated in figure 7 GBN13006, calcined at 1300°C/6h, has a considerably lower ability to convert CH_4 and syngas than GBN12006. Despite low methane conversion GBN12006 shows the best syngas conversion. By comparing the CH_4 and syngas conversion graphs of the Brazilian ore based sample sintered at 1200°C/6h (BRZ120012), it is seen that although this oxygen carrier has the lowest CH_4 conversion among all the tested samples it shows high syngas conversion.

3.1.3. Gas conversion of oxygen carriers with addition of Fe_2O_3

In order to find the most optimal sintering temperature/duration, several experiments on the four manganese ores (East European, South African (A)& (B), and Egyptian) with addition of Fe_2O_3 were conducted. First, South African (B) and East European ores with Mn:Fe molar ratio of 1:2 were sintered at 1100°C for 6 hours (SAFB2F11006, ESE2F11006). The methane conversion of these oxygen carriers was very poor (see figure 8a, 8b). For the second attempt, the sintering temperature and duration for these two samples were lowered to 950°C and 4 hours (SAFB2F9504, ESE2F9504). As seen in figure 8a and 8b lowering the sintering temperature/duration caused slight increase in their CH_4 conversion ability.

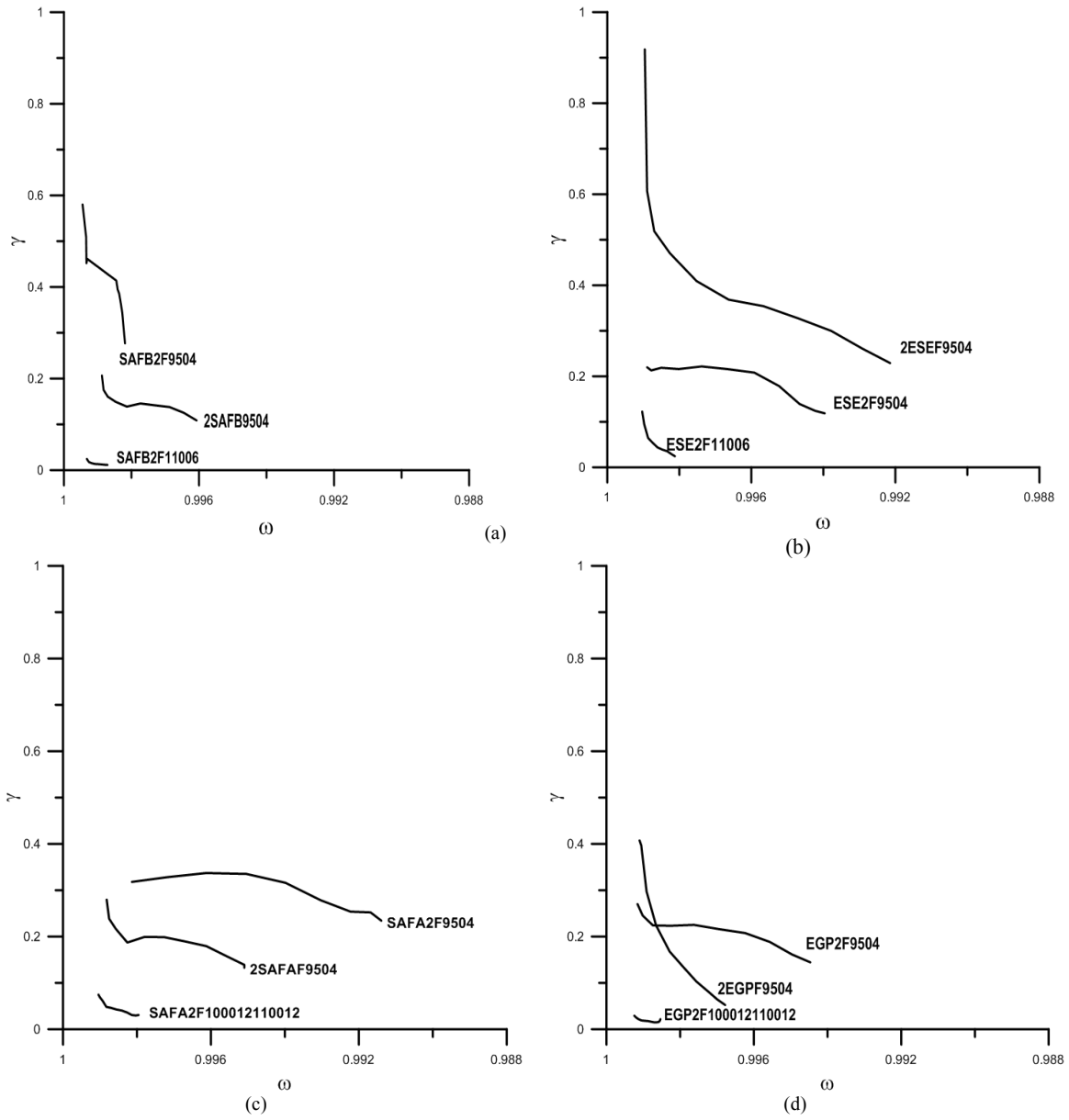

Figure 8-*Gas yield as a function of oxygen carrier mass-based conversion for different oxygen carriers based on a) SAFB, b) SAFA, c) ESE and d) EGP ores with addition of Fe_2O_3 during reduction with CH_4 as fuel at 950°C.*

As shown in figure 8c and 8d, the methane conversion of SAFA2F100012110012 and EGP2F100012110012 is very low. When the sintering step prior to the extrusion was excluded and the final temperature/duration decreased to 950°C/4h (SAFA2F9504 and EGP2F9504) the conversion ability of the samples considerably increased. So

temperature of 950°C and 4 hours was selected as the rather optimal sintering condition for these ores.

To investigate the Mn:Fe molar ratio in the oxygen carriers, the Mn:Fe molar ratio increased to 2:1. As it is illustrated in figure 8, different ores showed different behaviour for different ratios. For instance, East European ore–based sample, 2ESEF9504, showed high methane conversion. On the other hand, oxygen carriers made by the South African (A) & (B) and Egyptian ores (2SAFAF9504, 2SAFB9504 and 2EGPF9504 respectively) became less reactive when the added amount of iron oxide decreased.

Figure 9 presents the gas yield, γ, as a function of oxygen carrier conversion, ω, during reduction with CH_4 as fuel at 950°C for the six samples with Mn:Fe molar ratio of 1:2. As shown, the sample made from Brazilian ore (BRZ2F9504) shows the highest methane conversion. The Gabon-ore based sample (GBN2F9504) had the second highest CH_4 conversion at 950°C. Looking at Table 4, one can see that these two ores have very similar compositions. The other four samples have much lower methane conversion ability. Comparing figures 9 and 6, it is seen that conversion pattern of the oxygen carriers with addition of iron oxide is very different from the samples that have calcium hydroxide as the additive. For instance, the samples made by the South African (B) ore had the highest CH_4 conversion among the all samples with addition of $Ca(OH)_2$. But when iron oxide is added, South African (B) ore-based showed very low methane conversion ability. On the other hand, Gabon ore-based oxygen carrier was much more reactive when it was mixed with iron oxide instead of calcium hydroxide.

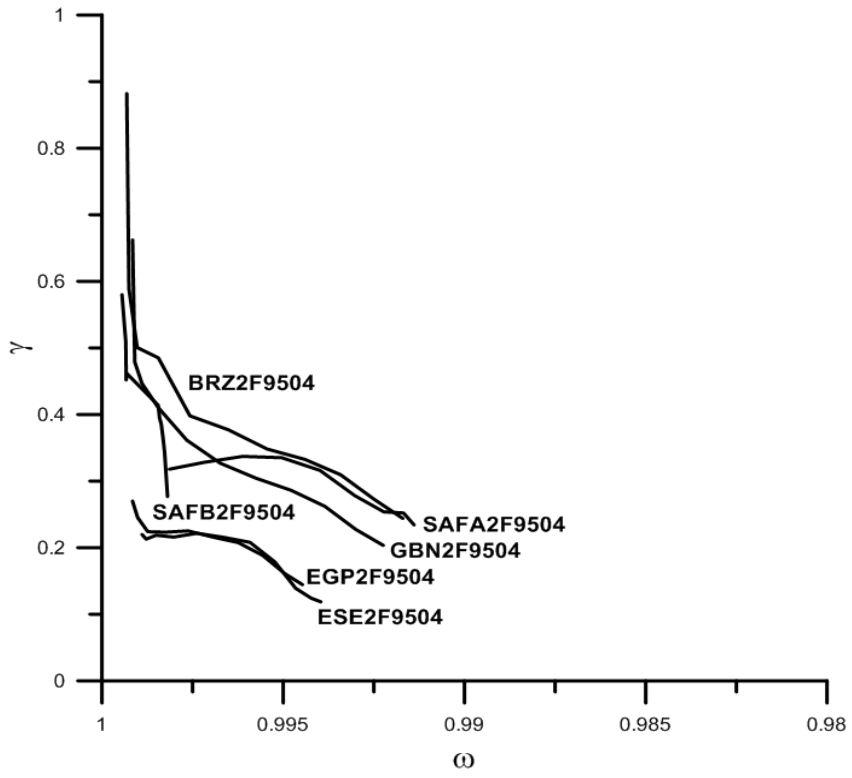

Figure 9- *Gas yield as a function of oxygen carrier mass-based conversion during reduction with CH_4 as fuel at 950°C for samples with Mn:Fe molar ratio of 1:2*

Graphs of the gas yield, γ, as a function of oxygen carrier conversion, ω, during reduction with CH_4 as fuel at 950°C for the six samples with Mn:Fe molar ratio of 2:1 are illustrated in figure 10. As shown, the oxygen carrier based on Brazilian ore (2BRZF9504) showed the highest conversion and had improved in compare to BRZ2F9504 (see figure 9). By decreasing the amount of the added iron oxide the methane conversion of the East European ore-based oxygen carrier (2ESEF9504) slightly improved. The behaviour of other samples follows almost the same trend as when the Mn:Fe molar ratio is 1:2 (figure 9). Comparing graphs in figure 9 and 10, it is seen that the reactivity of the oxygen carriers based on Brazilian, East European and Gabon ores increases by raising the share of manganese in the samples. On the other hand, when the share of manganese was increased in samples made by South African and Egyptian ores they became less reactive in terms of CH_4 conversion.

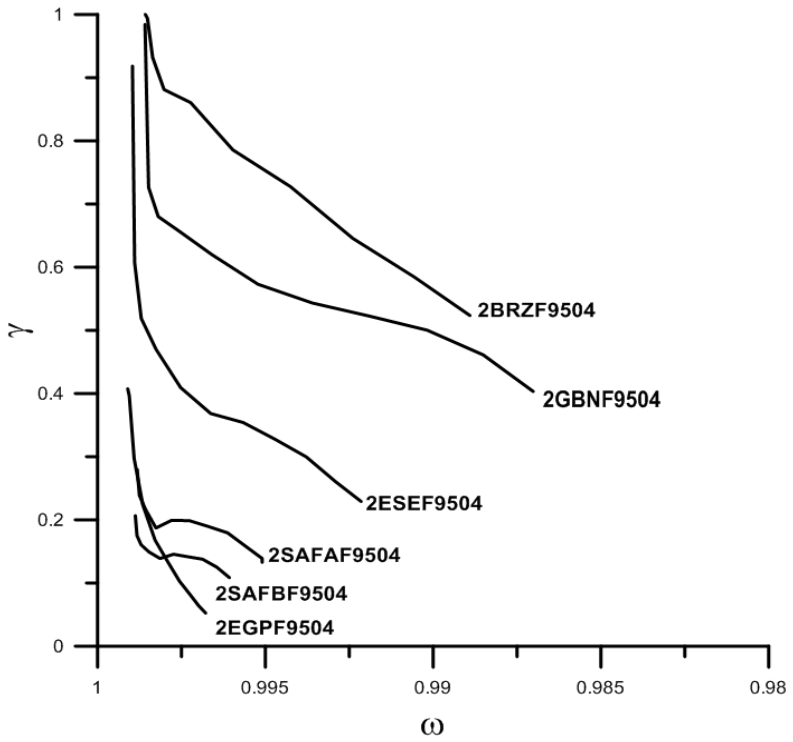

Figure 10- *Gas yield as a function of oxygen carrier mass-based conversion during reduction with CH_4 as fuel at 950°C for samples with Mn:Fe molar ratio of 2:1.*

No syngas experiment was conducted on the samples with addition of iron oxide.

3.2. Oxygen uncoupling behaviour

For all samples the release of oxygen in an inert atmosphere by exposing oxygen carriers to N_2 at 900°C was examined. Particles with high gaseous O_2 release during N_2 periods, the so called CLOU effect, can enhance solid fuel conversion [20].

3.2.1. Oxygen uncoupling behaviour of the pure managanese ores

Figure 11 presents O_2 release at 900°C as a function of oxygen carrier mass-based conversion, ω, for the six pure, untreated manganese ores. As shown, oxygen release level in the case of all the ores goes to zero. Their oxygen-carrier capability seems to be poor, which their Δω during 60 s of N_2 period seems to be less than 0.08%. Although East European ore, ESE, showed significantly better reactivity to convert CH_4 at 950°C (see figure 5), but its O_2 release ability at 900°C is no better than others.

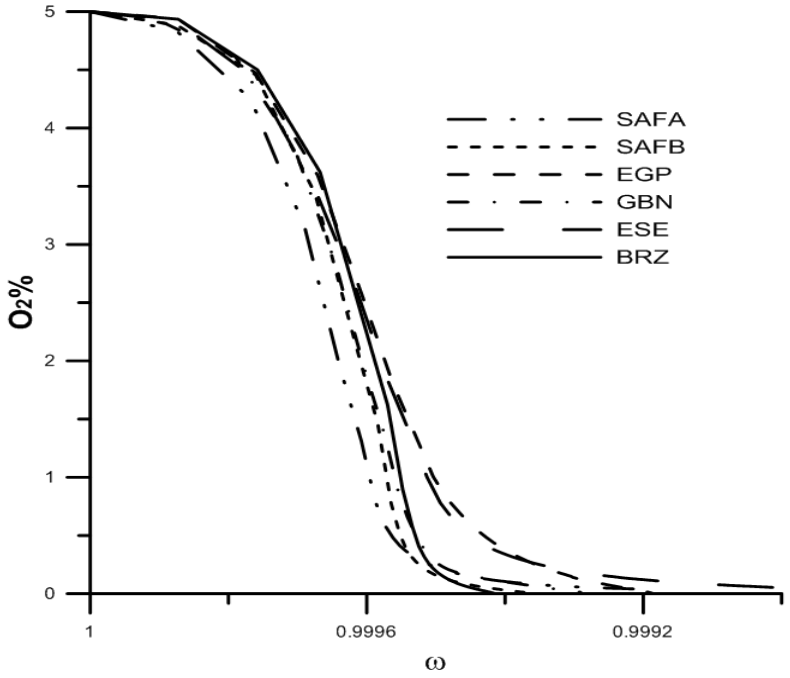

Figure 11-*Oxygen release as a function of oxygen carrier mass-based conversion during N_2 period at 900°C for the six pure, untreated manganese ores*

3.2.2. Oxygen uncoupling behaviour of the oxygen carriers addition of $Ca(OH)_2$

Unlike CH_4 conversion, O_2 release for different samples show less variation. Figure 12 presents O_2 release at 900°C as a function of oxygen carrier mass-based conversion, ω, for five samples of manganese ore with addition of $Ca(OH)_2$ sintered at 1300°C/6h. Comparatively the sample made from synthetic manganese oxide, SMN13006, releases the highest O_2 during the N_2 periods.

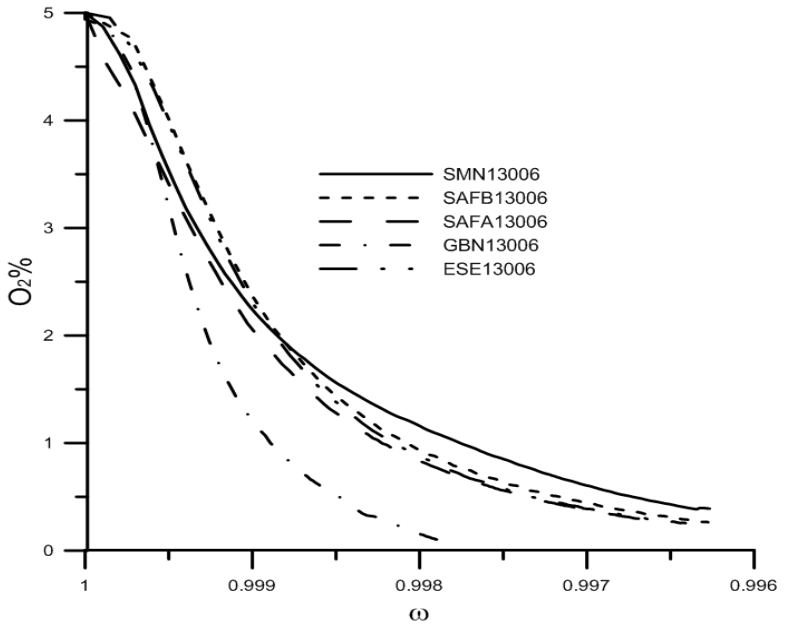

Figure 12- *Oxygen release as a function of oxygen carrier mass-based conversion during N_2 period at 900°C for the five samples of manganese ore with addition of ca(OH)$_2$ sintered at 1300°C/6h*

By comparing figure 6 and 12, one can see that although ESE13006 and SAFA13006 have lower CH_4 conversion than SAFB13006, their O_2 release capabilities seem to be equal (about 0.3%). As shown in figure 12, the mass-based conversion difference, Δω, of SAFA13006, SAFAB13006 and ESE13006 during the 360 seconds of N_2 period is approximately 0.4 %. On the other hand, Δω for the different oxygen carriers in CH_4 period is considerably higher, 0.5%-2.3% (see figure 6). As illustrated in figure 6, during the 20 seconds of CH_4 addition, Δω = 1.5% for SAFB13006, but for ESE13006 Δω = 0.75%. So all the samples lose much less oxygen during N_2 periods than in CH_4 cycles.

This is partly explained by the low equilibrium oxygen partial pressure that makes the O_2 release slow. It is also evident from figure 12 that most of the oxygen carriers still release O_2 after 360 s. Just as for CH_4 conversion, the samples made of Gabon Mn-ore (GBNs) shows the lowest oxygen release. Unlike CH_4 conversion, the oxygen release of the samples in N_2 periods didn't seem to be sensitive to change in calcination scheme.

3.2.3. Oxygen uncoupling behaviour of the Oxygen carriers with addition of Fe_2O_3

Figure 13 illustrates O_2 release at 900°C as a function of oxygen carrier mass-based conversion, ω, for the oxygen carriers with Mn:Fe molar ratio of 1:2 & 2:1 sintered at 950°C/4h. As seen, none of the oxygen carriers showed decent O_2 release at 900°C. However comparing the samples with different Mn:Fe molar ratio, one can see that mostly those with a higher iron share had slightly better performance in terms of O_2 release. The Brazilian, Gabon and Egyptian ore-based samples had very low O_2 release. Comparing methane conversion and O_2 release diagrams, one can see those oxygen carries with decent methane conversion like Brazilian or Gabon ore-based samples have very low oxygen release at 900°C. As seen in figures 13a and 13b, the mass-based conversion difference, Δω, of these samples during the 360 s of N_2 period regardless of their share of additive iron oxide release is less than 0.08%. Besides, their oxygen release level went to zero before the end of the N_2 period.

On the other hand, oxygen carriers made from South African (A) & (B) and East European ores with Mn:Fe molar ratio of 1:2 (see figure 13a) showed almost the same level of oxygen release in the N_2 periods equals to 0.2%. When the amount of added iron oxide to these ores decreased (Mn:Fe of 2:1, see figure 13b) their ability to oxygen release also decreased.

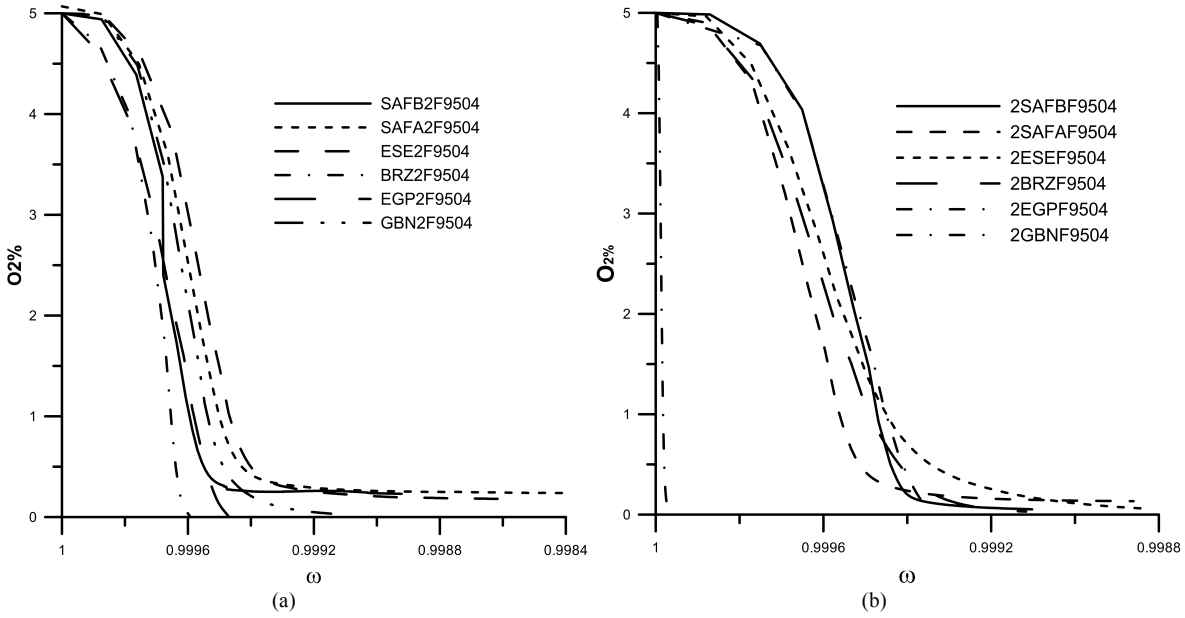

Figure 13- *Oxygen release as a function of oxygen carrier mass-based conversion during N_2 period at 900°C for the samples with nMn/nFe of a) 1:2 and b) 2:1, all sintered at 950°C/4h*

3.3. Solid fuel conversion

Solid fuel tests according to the conditions described in section 2.2 was done on the samples with the good reactivity during gaseous fuels experiments i.e. SAFB13006, SAFA13006 and ESE13006 from the samples with addition of $Ca(OH)_2$ (see figure 6) and BRZ2F9504, ESE2F9504 and GBN2F9504 from the samples with addition of Fe_2O_3 (see figure 9). The used Solid fuels were wood char in the case of samples with $Ca(OH)_2$ and devolatilized petroleum coke for samples with addition of Fe_2O_3.

3.3.1. Solid fuel conversion of the oxygen carriers with addition of $Ca(OH)_2$

In figure 14a-c the corrected outlet gas concentrations, i.e. dried concentration not including the sweep gas, are shown as a function of time for the reducing period for SAFA13006, SAFB13006 and ESE13006 particles with wood char at 950 °C. In all cases 10 g of oxygen carrier were used.

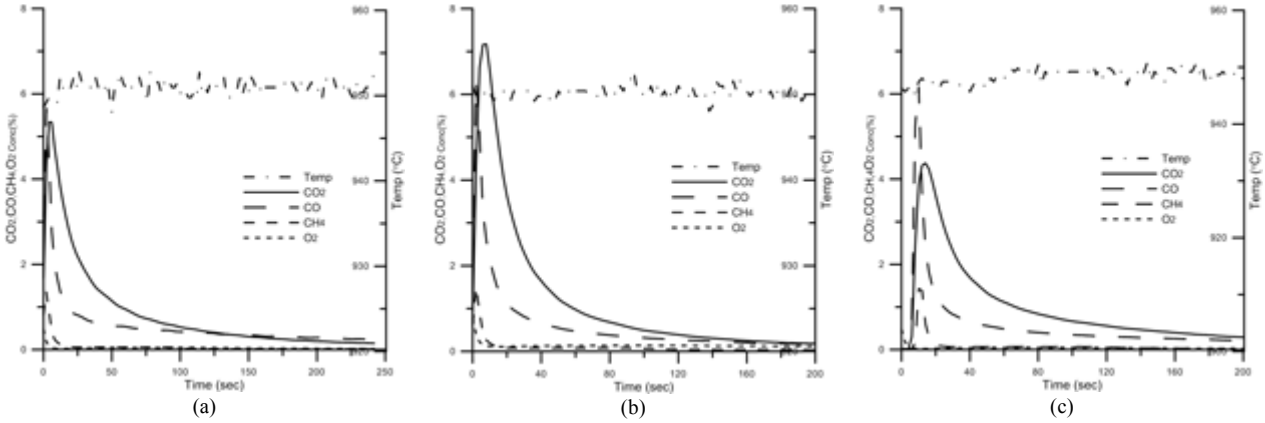

Figure 14- *Concentrations for the reduction for a cycle with 0.1 g of Swedish wood char in 10 g of (a) SAFB13006, (b) SAFA13006 and (c) ESE13006 oxygen carriers at 950 °C. The fluidizing gas in reduction is pure nitrogen.*

When the fuel is introduced to the reactor peaks of CH_4 and CO can be seen in the beginning of the reaction due to devolatilization of the fuel. Some volatiles react with the oxygen carrier and CO_2 increases rapidly. For all of the three oxygen carriers the peak value for CO_2 is almost the same as the peak for CO and higher than the CH_4 peak. The oxygen concentration falls to zero as the fuel conversion consumes all O_2 released. After

devolatilization is finished, the remaining char can only be converted by reaction with released oxygen from the oxygen carrier. This is because the fluidizing gas is nitrogen, so there is no or very little gasification. Thus, the CO_2 is a measure of the oxygen release.

Figure 15 illustrates the mass-based conversion as a function of time during the exposure to N_2 (60 sec) followed reduction by addition of 0.1 g wood char at 950°C. Calculating the $\Delta\omega$ when $\omega_{t=0}$ is the mass-based conversion of particles at the end of oxidation which is assumed to be equal to 1 gives a better understanding of the ability of the oxygen carriers to release oxygen in an reducing atmosphere at 950°C. In this case $\Delta\omega$, of SAFA13006, SAFB13006 and ESE13006 would be 0.68%, 0.62% and 0.37%, respectively (see figure 15). The fuel and oxidation periods in these experiments were separated by a period of N_2, so the particles release some part of their oxygen during this N_2 period prior to the fuel period. As seen, about 20 sec (for SAFA13006 and SAFB13006) to 60 sec (for ESE13006) after adding fuel the reactivity increase. That is due to the volatiles of the fuel, which accelerate the reaction rate. When devolatilization is finished the rate of reactions decreases and the slope becomes less steep.

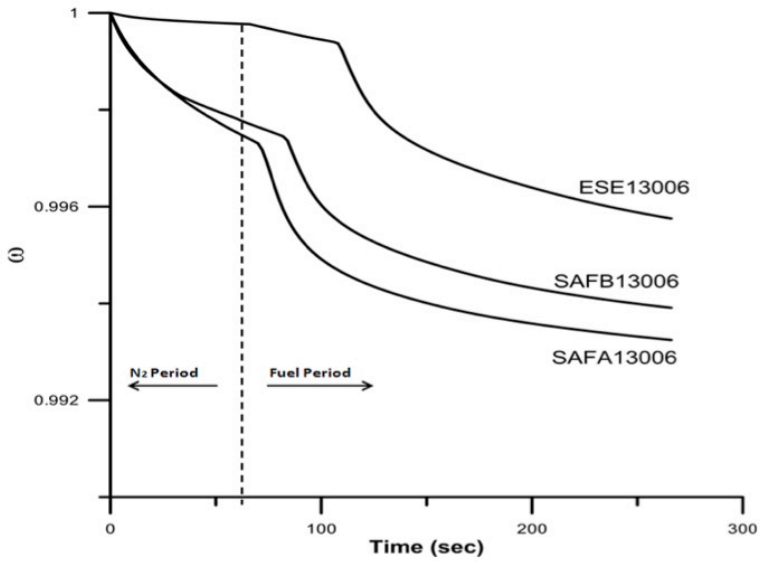

Figure 15- *Oxygen carrier mass-based conversion as a function of time during reduction with N_2 followed by addition of 0.1 g wood char at 950°C.*

3.3.2. Solid fuel conversion of the oxygen carriers with addition of Fe_2O_3

Figure 16a-c presents the corrected outlet gas concentrations, i.e. dried concentration not including the sweep gas, as a function of time for the reducing period for particles made from Brazilian, East European and Gabon ores and Fe_2O_3 with Mn:Fe molar ratio of 1:2, all sintered at 950°C/4h (BRZ2F9504, ESE2F9504 and GBN2F9504) with petroleum coke at 950 °C. In all cases 10 g of oxygen carrier were used.

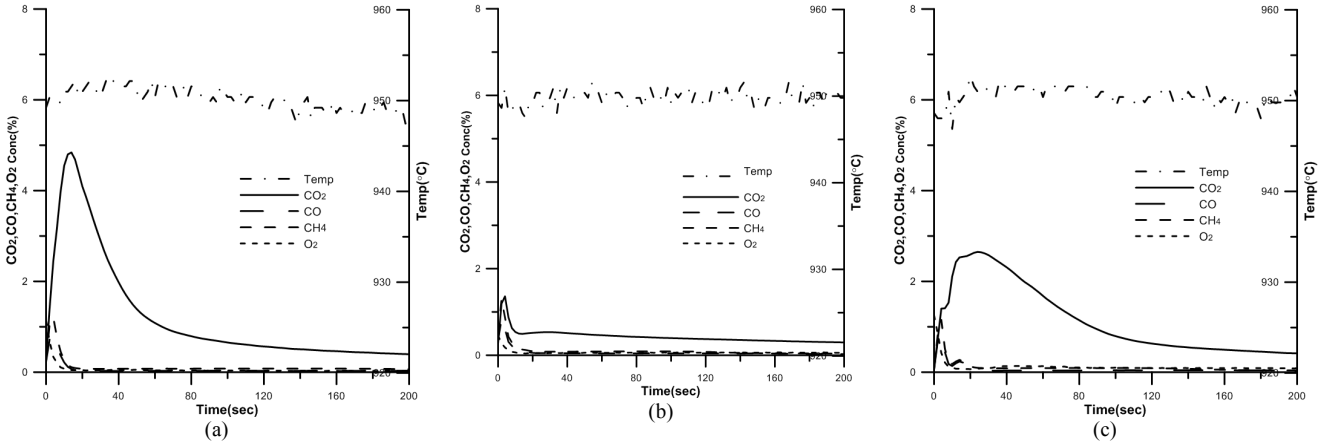

Figure 16- *Concentrations for the reduction for a cycle with 0.1 g of petroleum coke in 10 g of (a) BRZ2F9504, (b) ESE2F9504 and (c) GBN2F9504 oxygen carriers at 950 °C. The fluidizing gas in reduction is pure nitrogen.*

As seen, after 4 seconds of adding fuel, CH_4 and CO peaked. That is due to the immediate devolatilization of the fuel. Some of the released volatiles react with the oxygen carrier and the CO_2 concentration begins to increase. For BRZ2F9504 and GBN2F9504 the peak of CO_2 was reached with a 16 sec delay after CO and CH_4 (see figures 16a and 16c). On the other hand, in case of ESE2F9504 all the produced gases reached their peaks simultaneously (see figure 16b). In the beginning of the fuel periods temperature raised slightly (3-5°C) that could help to accelerate the conversion. For all the three samples after CO_2 reached its peak it took a very long time until the concentration felt to zero again i.e. the conversion was very slow. 20 seconds after the adding of the fuel the oxygen concentration falls to zero as the fuel consumes all the

released O_2.

The mass-based conversion of the three oxygen carriers as a function of time during the exposure to N_2 (60 sec) followed by reduction with addition of 0.1 g petroleum coke at 950°C is illustrated in figure 17.

As seen, Brazilian and Gabon ore based samples, BRZ2F9504 and GBN2F9504, had very similar mass based conversion behaviours. The $\Delta\omega$ throughout the N_2 period and its following pet coke period is 0.77% and 0.67% for BRZ2F9504 and GBN2F9504 respectively. The East European ore based sample, ESE2F9504, showed much less reactivity during the fuel experiment and its $\Delta\omega$ is 0.42%. One can see that the change of the slopes of the graphs in the N_2 period prior to the fuel period and when fuel is added to the reactor is insignificant (compare to figure 15). If the graphs' slope is a taken as an indication for reaction rate, it could be suggested that the reactivity of the particles doesn't seem to increase when fuel is added. One explanation could be the low release of the volatiles of the fuel (see figure 16), which is an important factor to accelerate the reactions and consumption of the released oxygen.

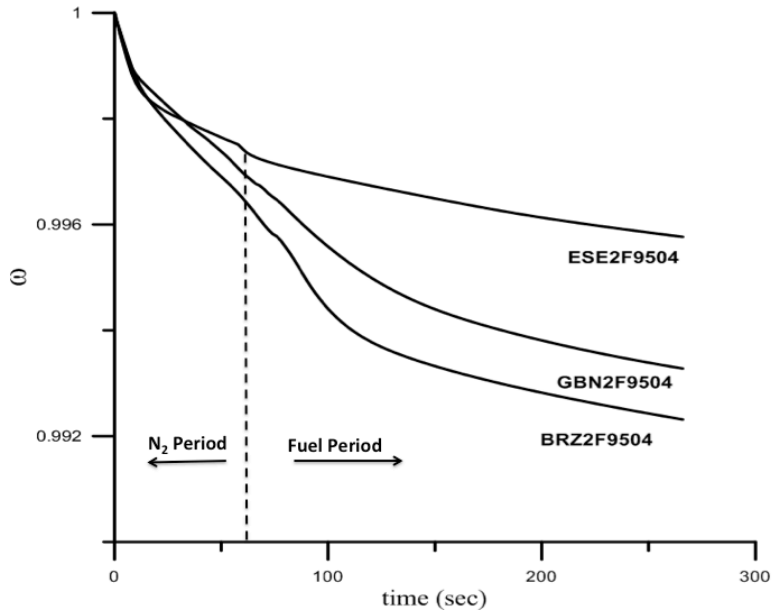

Figure 17- *Oxygen carrier mass-based conversion as a function of time during reduction with N_2 followed by addition of 0.1 g petroleum coke at 950°C.*

3.4. Oxygen carrier characterization

X-ray diffraction measurements were done on all the manufactured particles. The analysis of the phase compositions of the oxygen carrier particles was performed on a Siemens D5000 powder X-ray diffractometer (Cu Ka1, k = 1.54056 Å).

The shape and morphology of fresh and tested oxygen carriers were observed using a FEI, Quanta 200 Environmental Scanning Electron Microscope FEG.

The crushing strength, i.e. the force needed to fracture the particles, was examined using a Shimpo FGN-5 crushing strength apparatus. The mean value of the crushing strength for 30 particles in the range size of 180–212 μm is presented as the crushing strength value for each oxygen carrier. Fluidization property of the particles was verified by measuring the pressure drop in the reactor.

3.4.1. Characterisation of the oxygen carriers with addition of $Ca(OH)_2$

The X-ray diffractogram of samples made by manganese ores with addition of $Ca(OH)_2$ didn't reveal any considerable difference in phases formed at different calcination schemes of the same material. Besides, the X-ray diffractograms for most of the samples were almost identical, with detection of a major phase of cubic $CaMn_{(1-x)}Fe_xO_{3-\delta}$. Due to high iron oxide concentration in the Mn-ores and difficulties in distinguishing Fe from Mn, having major phase of $CaMn_{(1-x)}Fe_xO_{3-\delta}$ is not surprising (see Table 4). In the X-ray diffractograms of the untreated manganese-ores no $CaMn_{(1-x)}Fe_xO_{3-\delta}$ was found. These compositions had formed during the preparation procedures. Moreover, XRD results of synthetic manganese oxide samples (SMN13006, SMN12006) proved that the desired perovskite $CaMnO_{3-\delta}$ was formed. All the experiments ended with an oxidation phase and x-ray diffraction measurements on all the used samples were done as well. No significant phase change between the fresh and used particles was seen.

The Scanning Electron Microscopy, SEM, images of the samples were very similar hence only analysis of SAFB13006 in figure 18 is presented. One can see that the particles have a rough structure and their surface is porous both before and after the tests. Moreover, these images confirm that no evident changes in porosity or shape of the particles have taken place.

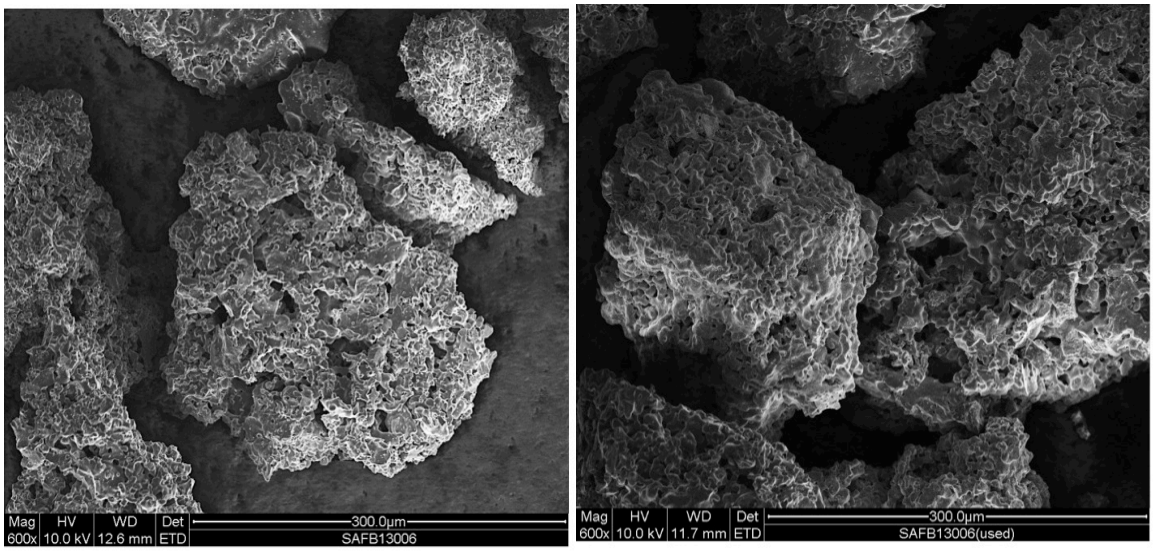

(a) (b)

Figure 18- *SEM images of SAFB13006 (a) prior to, (b) after the reactivity test. The images are 600x magnified at 300 µm range*

Table 7 presents the measured crushing strength of the particles after the experiment and fluidization properties of different materials at a temperature of 950°C. In Table 4, the fluidization behaviour is indicated by: 0 not defluidized; 1 temporarily defluidized or tendencies of defluidization; and 2 permanently defluidized during the experiment

Table 7-*Crushing strength and fluidization properties of all the samples with $Ca(OH)_2$.*

ID	Crushing strength (N)	Fluidization behaviour
SMN13006	3.0	0
SMN12006	1.9	0
GBN13006	2.2	0
GBN12006	1.4	1
ESE13006	2.4	0
ESE12506	1.4	1
ESE120012	1.2	1
ESE12006	1.3	2
SAFA13006	2.9	0
SAFA120012	1.6	0
SAFA12006	2.2	0
SAFB13006	2.4	0
SAFB12506	1.9	0
SAFB12006	1.5	0
BRZ13006	Melted	-
BRZ120012	1.0	1
EGP13006	1.8	2

3.4.2. Characterisation of the oxygen carriers with addition of Fe_2O_3

All the experiments on these samples were terminated in the reducing atmosphere using N_2. So it is assumed that the used particles are reduced and fresh particle are oxidized. Crushing strength and major detected phases of the fresh and used particles in the X-ray diffraction measurements are presented in Table 8. As seen, all the particles have decent crushing strength. Moreover, particles with higher iron oxide share showed higher crushing strength.

As illustrated in Table 8, the detected phases in all the fresh particles are mainly oxidized forms of iron oxide, manganese oxide or iron manganese oxide. The major detected phase in the used particles are reduced forms of iron manganese oxides $(Mn,Fe)_3O_{4-y}$. During the experiments none of the samples had any tendency for defluidization.

Table 8-*Crushing strength and XRD detected phases of the fresh and used samples with Fe_2O_3*

Samples	Crushing strength (N)	Fresh phase	Used phase
SAFB2F	3.41	Fe_2O_3 $(Mn,Fe)_2O_3$	$Mn_{0.43}Fe_{2.57}O_4$ $Mn_{1.88}Fe_{1.12}O_4$
2SAFBF	3.24	Mn_2O_3 $(Mn,Fe)_3O_4$	$Mn_{1.7}Fe_{1.3}O_4$
SAFA2F	3.67	$FeMnO_3$ Fe_2O_3	$Mn_{1.167}Fe_{1.33}O_4$
2SAFAF	2.86	$(Mn,Fe)_2O_3$ Fe_2O_3	$Mn_{0.97}Fe_{2.03}O_{3.95}$
ESE2F	2.83	$(Mn,Fe)_2O_3$	$Mn_{0.176}Fe_{1.1824}O_3$ $Mn_{1.5}Fe_{1.5}O_4$
2ESEF	2.79	$(Mn,Fe)_2O_3$	$Mn_{0.97}Fe_{2.03}O_{3.95}$
EGP2F	2.89	$(Mn,Fe)_2O_3$	$Mn_{0.97}Fe_{2.03}O_{3.95}$
2EGPF	2.26	$(Mn,Fe)_2O_3$	$Mn_{0.98}Fe_{2.02}O_4$
GBN2F	2.28	$(Mn,Fe)_2O_3$ Fe_2O_3	$Mn_{0.61}Fe_{1.39}O_4$
2GBNF	2.56	$Mn,Fe)_3O_4$ Fe_2O_3	$MnFe_2O_4$ $Mn_{1.03}Fe_{1.97}O_4$
BRZ2F	2.68	$FeMnO_3$ Fe_2O_3	$MnFe_2O_4$ $Mn_{1.03}Fe_{1.97}O_4$
2BRZF	2.60	$(Mn,Fe)_2O_3$ $Fe_{1.987}O_3$	$MnFe_2O_4$ $Mn_{1.28}Fe_{1.72}O_4$

4. Discussion

Among all the Mn-ore-based samples with addition of $Ca(OH)_2$, the South African (B) materials showed the highest CH_4 conversion, whereas, Gabon and Brazilian manganese ore-based samples showed the lowest methane conversion. These ores contain high around 5.19-5.84 wt% Si and around 3.26-4.05 wt% of Al. High concentration of Al could result in formation of manganese aluminate, which due to thermodynamic restrictions cannot be re-oxidized at the operating temperature (950°C) and pressure (P_{O2}=5%) [31].

The many impurities in the ores' make their behaviour very complex and difficult to explain. However, those ores with rather similar compositions seem to show similar behaviours. For instance, both Brazilian and Gabon ores have almost the same amount of Si, Al and Fe (see Table 4). Consequently, they had very similar CH_4 conversion, oxygen release, crushing strength and detected phases with both addition of $Ca(OH)_2$ and Fe_2O_3.

Comparing gas conversion of pure ores (figure 5) and the samples with $Ca(OH)_2$ sintered at 1300°C/6h presented in figure 6, one can see that the reactivity of most of the oxygen carriers in terms of CH_4 conversion has increased considerably. But in the case of East European manganese-ore–based sample, ESE13006, the proposed method seems to don't have any considerable effect on its reactivity.

However, comparing methane conversion of the pure ores and the samples with two different iron oxide mixtures, one could see that except for Brazilian and Gabon ore-based samples other oxygen carriers showed no considerable improvement. In the case of East European ore, when it was mixed with iron oxide with Mn:Fe molar ratio of 1:2 its reactivity dropped significantly. Comparing with their pure ores, the samples made form Brazilian and Gabon ores with M:Fe molar ratio of 1:2 and 2:1 sintered at 950°C/4h, (BRZ2F9504, 2BRZF9504, GBN2F9504 and 2GBNF9504) showed significant improvements in terms of methane conversion. The pure, untreated Brazilian and Gabon ore could release oxygen corresponding to 0.03% of their mass during the 20 sec of the CH_4 period at 950°C (see figure 5).

Azimi et.al tested oxygen carriers made from synthetic manganese and iron oxides manufactured by spray drying with different molar ratios under the same experimental conditions applied in this thesis [4]. In that work, there were huge differences in behaviour of oxygen carriers with Mn:Fe molar ratio of 1:2 and 2:1. Particles with Mn:Fe molar ratio of 1:2 were able to release oxygen equivalent to 1.4% of their mass when exposed to CH_4 at 950°C. They were also able to release 0.5% oxygen in the N_2 periods at 900°C. Whereas, particles with Mn:Fe molar ratio of 2:1 were much less reactive at 950°C and couldn't release any gaseous oxygen during N_2 period at 900°C .

On the contrary, oxygen carriers made by manganese ores and iron oxide with Mn:Fe molar ratio of 1:2 showed very similar characteristics to the samples with the same ores and iron oxide but with Mn:Fe molar ratio of 2:1. (See figures 9,10 and 13).

In this work ESE-samples prepared in the same way showed inconsistent results. Energy-dispersive X-ray spectroscopy, EDX, analysis performed on ESE-samples showed there were inhomogeneities in chemical characterization of ESE-samples prepared by identical methods. Although the variations were slight (=<1 wt%) this may have noticeable impact on the samples' performance. One drawback of ore-based oxygen carriers is that not all of them are well homogenized. Having even small heterogeneity in ores would affect their reproducibility.

During the solid fuel tests both with wood char and petroleum coke, devolatilization of the fuels occurs during 10 seconds after the fuels was added to the reactor, see peaks of CH_4 in figures 14 and 16. Looking at figure 15, it seen that the slope of the curves become more steep during this period, which corresponds to a $\Delta\omega$ of 0.1-0.15%. In solid fuel tests with petroleum coke (see figure 17) the oxygen release in the 10 seconds period of the fuel devolatilization is equivalent to a $\Delta\omega$ of 0. 05-0.16%. There are three possibilities;

i) The lowering of the oxygen concentration caused by the volatiles is sufficient to make the oxygen carrier release oxygen more rapidly, i.e. there is no direct reaction

ii) The volatiles consume oxygen more rapidly than it can be released, and reacts directly with the oxygen carrier

iii) A mixture of both i) and ii)

Thus some share of oxygen release in the fuel periods could be due to the direct reaction of volatiles, although for some particles it is insignificant. However, looking at the figures 15 and 17 it is seen that after this devolatilization period particles continue to release considerable amount of oxygen.

5. Conclusion

Oxygen carriers were manufactured from six different manganese ores with addition of calcium hydroxide or iron oxide using an extrusion method. Conversion of CH_4 and syngas as well as O_2 release of the oxygen carriers was investigated. Among all the tested Mn-ore-based samples with addition of calcium hydroxide, oxygen carriers based on South African-B manganese-ore sintered at 1300°C/6h showed the best results in terms of oxygen release and CH_4 conversion. All the oxygen carriers showed good syngas conversion. Oxygen carrier manufactured from Brazilian ore with Mn/Fe molar ratio of 2:1 sintered at 950°C/4h had the most promising CH_4 conversion among the all samples with addition of iron oxide. Solid fuel tests with wood char were conducted with oxygen carriers based on South African-B, South African-A and East European manganese-ores with addition of calcium hydroxide sintered at 1300°C/ 6h. These samples released an amount of oxygen corresponding to 0.37 to 0.68% of their mass

Besides, particles of Brazilian, Gabon and East European manganese-ore with addition of iron oxide with Mn:Fe molar ratio of 1:2 sintered at 950°C/4h were tested in solid fuel experiments using petroleum coke as the fuel. These samples were able to release oxygen corresponds to 0.42-0.77 wt%.

All the manufactured particles showed decent crushing strength and most of them showed good fluidizability during the experiments. There was some variation in composition of the studied manganese- ores, which is the likely explanation to significant differences in their properties and reactivity. The work shows that calcium manganate and manganese iron oxide oxygen carriers can be manufactured by low cost ores, albeit with varying loss of reactivity compared to using the pure raw materials.

6. Acknowledgement

I would like to express my deepest gratitude to my supervisors Henrik Leion and Golnar Azimi for their support and precise supervision. My special appreciation goes to my examiner, Anders Lyngfelt, who provided me with the opportunity to work with the CLC group. I thank all the members of the CLC group for their friendly helps. My greatest thanks to my family for their supports and encouragement. Last but not least, I'd like to dedicate this work to my mother for her love and devotion.

7. References

1 J. Adanez, A. Abad, F. Garcia-Labiano, P. Gayan, and L. F. de Diego, 'Progress in Chemical-Looping Combustion and Reforming Technologies', *Progress in Energy and Combustion Science,* 38 (2012), 215-82.

2 J. Adanez, L. F. de Diego, F. Garcia-Labiano, P. Gayan, A. Abad, and J. M. Palacios, 'Selection of Oxygen Carriers for Chemical-Looping Combustion', *Energy & Fuels,* 18 (2004), 371-77.

3 A. Hedayati, A.M. Azad, M. Rydeń, H. Leion and T. Mattisson, 'Evaluation of Novel Ceria-Supported Metal Oxides as Oxygen Carriers for Chemical-Looping Combustion', *Industrial & Engineering Chemistry Research,* 51 (2012), 12796−806.

4 G. Azimi, H. Leion, T. Mattisson, and A. Lyngfelt, 'Chemical-Looping with Oxygen Uncoupling Using Combined Mn-Fe Oxides, Testing in Batch Fluidized Bed', *Energy Procedia,* 4 (2011), 370-77.

5 G. Azimi, H. Leion, T. Mattisson, and A. Lyngfelt, 'Chemical-Looping with Oxygen Uncoupling Using Combined Mn-Fe Oxides, Testing in Batch Fluidized Bed', *10th International Conference on Greenhouse Gas Control Technologies,* 4 (2011), 370-77.

6 G. Azimi, M. Rydén, H. Leion, T. Mattisson, and A. Lyngfelt, '(Mnzfe1−Z)Yox Combined Oxides as Oxygen Carrier for Chemical ‐ Looping with Oxygen Uncoupling (Clou)', *AIChE Journal* (2012).

7 P. Cho, T. Mattisson, and A. Lyngfelt, 'Comparison of Iron-, Nickel-, Copper- and Manganese-Based Oxygen Carriers for Chemical-Looping Combustion', *Fuel,* 83 (2004), 1215-25.

8 S. Y. Chuang, J. S. Dennis, A. N. Hayhurst, and S. A. Scott, 'Development and Performance of Cu-Based Oxygen Carriers for Chemical-Looping Combustion', *Combustion and Flame,* 154 (2008), 109-21.

9 C. Dueso, M. Ortiz, A. Abad, F. Garcia-Labiano, L. F. de Diego, P. Gayan, and J. Adanez, 'Reduction and Oxidation Kinetics of Nickel-Based Oxygen-Carriers for Chemical-Looping Combustion and Chemical-Looping Reforming', *Chemical Engineering Journal,* 188 (2012), 142-54.

10 H. Mantripragada, E. S. Rubin , A. Marks , P. Versteeg and J. Kitchin 'Review-the Outlook for Improved Carbon Capture Technology', *Progress in Energy and Combustion Science* (2012).

11 T. Norby, E. Bakken and S. Stolen, 'Nonstoichiometry and Reductive Decomposition of Camno3−Delta', *Solid State Ionics* 176 (2004), 217–23.

12 A. Fossdal, E. Bakken, B. A. Oye, C. Schoning, I. Kaus, T. Mokkelbost, and Y. Larring, 'Study of Inexpensive Oxygen Carriers for Chemical Looping Combustion', *International Journal of Greenhouse Gas Control,* 5 (2011), 483-88.

13 P. Gayan, C. R. Forero, L. F. de Diego, A. Abad, F. Garcia-Labiano, and J. Adanez, 'Effect of Gas Composition in Chemical-Looping Combustion with Copper-

Based Oxygen Carriers: Fate of Light Hydrocarbons', *International Journal of Greenhouse Gas Control,* 4 (2010), 13-22.

14 L. Al-Makhadmeh, G. Scheffknecht, U. Schnell and J Maier 'Oxy-Fuel Coal Combustion—a Review of the Current State-of-the-Art', *International Journal of Greenhouse Gas Control* (2011).

15 M. Wahlberg and J.S, Lindeløv, 'Spray Drying for Processing of Nanomaterials,International Conference on Safe Production and Use of Nanomaterials', *Journal of Physics: Conference Series 170* (2009).

16 M. Johansson, T. Mattisson, and A. Lyngfelt, 'Investigation of Mn3o4 with Stabilized Zro2 for Chemical-Looping Combustion', *Chemical Engineering Research & Design,* 84 (2006), 807-18.

17 M. E. M. Jorge, A. C. dos Santos, and M. R. Nunes, 'Effects of Synthesis Method on Stoichiometry, Structure and Electrical Conductivity of Camno3-Delta', *International Journal of Inorganic Materials,* 3 (2001), 915-21.

18 'Kyoto Protocol to the United Nations Framework Convention on Climate Change 1998'.

19 H. Leion, T. Mattisson, and A. Lyngfelt, 'Use of Ores and Industrial Products as Oxygen Carriers in Chemical-Looping Combustion', *Energy & Fuels,* 23 (2009), 2307-15.

20 H. Mattisson Leion, T. Lyngfelt, A., 'Using Chemical-Looping with Oxygen Uncoupling (Clou) for Combustion of Six Different Solid Fuels', *Greenhouse Gas Control Technologies 9,* 1 (2009), 447-53.

21 A. Lyngfelt, B. Leckner, and T. Mattisson, 'A Fluidized-Bed Combustion Process with Inherent Co2 Separation; Application of Chemical-Looping Combustion', *Chemical Engineering Science,* 56 (2001), 3101-13.

22 M. Rydén, A. Lyngfelt and T. Mattisson, 'Camn0.875ti0.125o3 as Oxygen Carrier for Chemical-Looping Combustion with Oxygen Uncoupling (Clou)—Experiments in a Continuously Operating Fluidized-Bed Reactor System', *International Journal of Greenhouse Gas Control,* Volume 5 (2011), Pages 356–66.

23 T. Mattisson, A. Lyngfelt, and H. Leion, 'Chemical-Looping with Oxygen Uncoupling for Combustion of Solid Fuels', *International Journal of Greenhouse Gas Control,* 3 (2009), 11-19.

24 B. Metz, O. Davidson, H. C. de Coninck, M. Loos, and L. A. Meyer, 'Ipcc, 2005: Ipcc Special Report on Carbon Dioxide Capture and Storage. Prepared by Working Group Iii of the Intergovernmental Panel on Climate Change', *Cambridge, United Kingdom and New York, NY, USA, 442 pp* (2005).

25 'Mineral Commodity Summaries. U.S. Geological Survey', (2010).

26 J. C. M. Pires, F. G. Martins, M. C. M. Alvim-Ferraz, and M. Simoes, 'Recent Developments on Carbon Capture and Storage: An Overview', *Chemical Engineering Research & Design,* 89 (2011), 1446-60.

27 M. Ryden, A. Lyngfelt, and T. Mattisson, 'Combined Manganese/Iron Oxides as Oxygen Carrier for Chemical Looping Combustion with Oxygen Uncoupling (Clou) in a Circulating Fluidized Bed Reactor System', *10th International Conference on Greenhouse Gas Control Technologies,* 4 (2011), 341-48.

28 D.L. Segal, 'Sol-Gel Processing: Routes to Oxide Ceramics Using Colloidal Dispersions of Hydrous Oxides and Alkoxide Intermediates', *Journal of Non-Crystalline Solids,* 63 (1984,).
29 A. Shulman, E. Cleverstam, T. Mattisson, and A. Lyngfelt, 'Chemical - Looping with Oxygen Uncoupling Using Mn/Mg-Based Oxygen Carriers - Oxygen Release and Reactivity with Methane', *Fuel,* 90 (2011), 941-50.
30 E. R. Stobbe, B. A. de Boer, and J. W. Geus, 'The Reduction and Oxidation Behaviour of Manganese Oxides', *Catalysis Today,* 47 (1999), 161-67.
31 A. Ja¨rdna¨s, T. Mattisson and A. Lyngfelt, 'Reactivity of Some Metal Oxides Supported on Alumina with Alternating Methane and Oxygensapplication for Chemical-Looping Combustion', *Energy & Fuels,* 17 (2003), 643-51.
32 D. G. Wang, F. Guo, J. F. Chen, R. H. Zhao, and Z. T. Zhang, 'Synthesis of Nano-Platelets of Modified Aluminium Hydroxide by High-Gravity Reactive Precipitation and Hydrothermal Method', *Materials Chemistry and Physics,* 107 (2008), 426-30.
33 K. Teong, L. Zhi, H. Lee, S. Bhatia and A.R. Mohamed, 'Post-Combustion Carbon Dioxide Capture: Evolution Towards Utilization of Nanomaterials', *Renewable and Sustainable Energy Reviews,* 16 (2012), 2599-609.